NIH Public Access
Author Manuscript
J Comp Neurol. Author manuscript; available in PMC 2013 February 15.

Published in final edited form as:
J Comp Neurol. 2012 September 1; 520(13): 2888–2902. doi:10.1002/cne.23070.

Morphologic Evidence for Spatially Clustered Spines in Apical Dendrites of Monkey Neocortical Pyramidal Cells

Aniruddha Yadav[1,2], **Yuan Z. Gao**[1,2], **Alfredo Rodriguez**[1,2], **Dara L. Dickstein**[1,2], **Susan L. Wearne**[1,2,†], **Jennifer I. Luebke**[3], **Patrick R. Hof**[1,2], and **Christina M. Weaver**[2,4,*]

[1]Fishberg Department of Neuroscience and Friedman Brain Institute, Mount Sinai School of Medicine, New York, New York 10029

[2]Computational Neurobiology and Imaging Center, Mount Sinai School of Medicine, New York, New York 10029

[3]Department of Anatomy and Neurobiology, Boston University School of Medicine, Boston, Massachusetts 02118

[4]Department of Mathematics, Franklin and Marshall College, Lancaster, Pennsylvania 17604

Abstract

The general organization of neocortical connectivity in rhesus monkey is relatively well understood. However, mounting evidence points to an organizing principle that involves clustered synapses at the level of individual dendrites. Several synaptic plasticity studies have reported cooperative interaction between neighboring synapses on a given dendritic branch, which may potentially induce synapse clusters. Additionally, theoretical models have predicted that such cooperativity is advantageous, in that it greatly enhances a neuron's computational repertoire. However, largely because of the lack of sufficient morphologic data, the existence of clustered synapses in neurons on a global scale has never been established. The majority of excitatory synapses are found within dendritic spines. In this study, we demonstrate that spine clusters do exist on pyramidal neurons by analyzing the three-dimensional locations of ~40,000 spines on 280 apical dendritic branches in layer III of the rhesus monkey prefrontal cortex. By using clustering algorithms and Monte Carlo simulations, we quantify the probability that the observed extent of clustering does not occur randomly. This provides a measure that tests for spine clustering on a global scale, whenever high-resolution morphologic data are available. Here we demonstrate that spine clusters occur significantly more frequently than expected by pure chance and that spine clustering is concentrated in apical terminal branches. These findings indicate that spine clustering is driven by systematic biological processes. We also found that mushroom-shaped and stubby spines are predominant in clusters on dendritic segments that display prolific clustering, independently supporting a causal link between spine morphology and synaptic clustering.

INDEXING TERMS

clustering; dendritic spines; plasticity; morphology; image analysis

A large body of theoretical and experimental evidence points to synaptic clustering as a basic organizing principle of neuronal connectivity. Theoretical models have shown that

© 2012 Wiley Periodicals, Inc.

*CORRESPONDENCE TO: Christina M. Weaver, Department of Mathematics, Franklin and Marshall College, P.O. Box 3003, Lancaster, PA 17604-3003. christina.weaver@fandm.edu.

†We dedicate this article to Susan L. Wearne, our friend, colleague, and mentor, who passed away in September, 2009.

NIH-PA Author Manuscript
NIH-PA Author Manuscript
NIH-PA Author Manuscript

NIH-PA Author Manuscript

NIH-PA Author Manuscript

NIH-PA Author Manuscript

precisely timed and spatially localized synaptic inputs can sum nonlinearly (Mehta, 2004; Govindarajan et al., 2006; Larkum and Nevian, 2008), generating a response that is either greater or less than expected if the inputs were simply added together. Nonlinear summation of synaptic inputs increases a neuron's flexibility to differentiate spatiotemporal input patterns and greatly enhances its computational efficiency (Poirazi and Mel, 2001; Poirazi et al., 2003; Polsky et al., 2004; Gordon et al., 2006). Such nonlinear summation in spatially localized synapses has also been observed experimentally (Larkum and Nevian, 2008; Larkum et al., 2009). Important new evidence suggests that groups of spatially localized synapses on a dendrite can process functionally similar information from presynaptic cell assemblies (Takahashi et al., 2012).

It has also been reported that newly formed spines preferentially grow near synapses activated through learning-related induction of long-term potentiation (LTP), possibly leading to spine clustering (De Roo et al., 2008). Recent experiments have also suggested that the spatially colocalized synapses can be regulated simultaneously and provide a mechanistic framework that could account for the emergence of spatial synapse clusters. Harvey and Svoboda found that early-phase LTP (E-LTP) induction at one synapse lowered the threshold for E-LTP induction at synapses within a ~10-μm neighborhood on the same dendrite branch (Harvey and Svoboda, 2007). Specifically, Harvey and Svoboda showed that protein-synthesis-independent cross-talk between a synapse and its neighbors existed after induction of E-LTP. Govindarajan and colleagues (2011) studied the protein-synthesis-dependent late phase of LTP (L-LTP) and demonstrated that the efficiency of L-LTP induction on a dendritic spine neighboring a spine in which LTP had already been induced was inversely proportional to the distance between the two spines. Further support for clustered synapses arises from the existence of dendritic spikes, which are likely to be evoked by spatiotemporally localized synaptic inputs (Larkum et al., 2001; Murayama et al., 2007).

Despite these clues, the question of whether synapse clustering occurs on a global scale on branches throughout the dendritic arbor is difficult to explore. Several network-level approaches are able to identify synaptic connections between specific neurons. Recent technologies, including light-activated ion channels (Petreanu et al., 2007), glutamate uncaging (Nikolenko et al., 2007), trans-synaptic tracers (Wickersham et al., 2007), genetic labeling (Livet et al., 2007), and in vivo multiphoton imaging (Kerr and Denk, 2008), have made great strides in improving our understanding of how neurons connect to form circuits. However, identifying individual synapses participating in these connections and determining whether synapses group together functionally to transmit related information falls beyond the purview of these technologies.

There is much to be gained by examining the location and distribution of synapses on individual neurons. On many neurons, dendritic spines provide a morphologic reflection of the presence of excitatory synapses. Confocal and multiphoton laser scanning microscopy (for review see Wilt et al., 2009) have allowed us to visualize spines across entire neurons, making analysis of the three-dimensional (3-D) spine shape and location theoretically possible. However, manual analysis of spines is prohibitively time consuming and widely subject to operator variability. Recent software packages now can analyze dendrite and spine morphology automatically (for review see Lemmens et al., 2010; Meijering, 2010), greatly reducing manual interventions to initial setup and postanalysis editing. In particular, we utilized NeuronStudio (Rodriguez et al., 2003, 2006, 2008, 2009; Dumitriu et al., 2011) for all automated morphology reconstructions included in this study. Still, establishing the existence and biological significance of clusters of spines is inherently problematic. Visual inspection may identify clusters but cannot differentiate between clustering resulting from a systematic biological process and clustering that occurs purely by chance. As automated

NIH-PA Author Manuscript

NIH-PA Author Manuscript

NIH-PA Author Manuscript

image analysis methods render high-resolution morphologic data more accessible, we need a subjective method to test whether spine clustering occurs more often than expected by chance.

Here we present a novel approach that pairs a clustering algorithm with Monte Carlo simulations to perform such a test. We introduce a measure called the "C-score," which is independent of spine density and quantifies the probability that the observed number of spine clusters occurred randomly. We analyzed the spatial location and shape of spines from 280 dendrite branches of seven layer III prefrontal cortex (PFC) pyramidal neurons from three adult rhesus monkeys, imaged in their entirety at high resolution. We show that the frequency of spine clustering on apical terminal branches of these neurons is unlikely to occur merely by chance, suggesting that a systematic biological process contributes to the observed clustering. We also found that clusters have higher densities of mushroom-shaped and stubby spines on dendrites with prolific clustering than on dendrites with sparse clustering, indicating that spine shape and clustering may be coregulated.

MATERIALS AND METHODS

Cell imaging, 3-D neuron reconstruction, and morphometric analysis

Seven layer III pyramidal neurons filled during electrophysiological recordings in in vitro slices prepared from the dorsolateral PFC (area 46) of three young adult male rhesus monkeys (*Macaca mulatta*, ages ranging from 5.2 to 6.9 years) were used in the present study. These materials were derived from animals killed as part of other ongoing studies involving a larger set of subjects. These three monkeys were part of a cohort used in studies of normal aging on the brain. Animals were behaviorally assessed on a battery of cognitive tasks (Chang et al., 2005; Luebke and Amatrudo, 2010), but no invasive procedures had been performed on them prior to the time of death.

The monkeys were housed at the Boston University Laboratory Animal Science Center (LASC) in strict accordance with animal care guidelines as outlined in the NIH *Guide for the care and use of laboratory animals* and the U.S. Public Health Service policy on humane care and use of laboratory animals. Boston University LASC is fully accredited by the Association for Assessment and Accreditation of Laboratory Animal Care, and all procedures were approved by the Institutional Animal Care and Use Committee (IACUC). Electrophysiological and cell filling protocols were performed as described in detail elsewhere (Luebke and Chang, 2007; Luebke and Amatrudo, 2010).

Ketamine (10 mg/ml) was used to tranquilize the monkeys, following which they were deeply anesthetized with sodium pentobarbital (to effect 15 mg/kg, i.v.). Next, the monkeys underwent a thoracotomy, and a craniotomy was performed. A biopsy was conducted to obtain 10-mm-thick blocks of the PFC (area 46) containing both the upper and lower banks of the principal sulcus. A vibrating microtome was used to cut 400-μm-thick coronal slices, which were placed in 26°C oxygenated (95% O_2/5% CO_2) Ringer's solution (concentrations in mM: 26 $NaHCO_3$, 124 NaCl, 2 KCl, 3 KH_2PO_4, 10 glucose, 2.5 $CaCl_2$, 1.3 $MgCl_2$, pH 7.4; all chemicals obtained from Sigma, St. Louis, MO). Slices equilibrated for at least 1 hour and were maintained for up to 12 hours. The time between perfusion and PFC slice preparation was approximately 10–15 minutes. For recording, individual slices were positioned under a nylon mesh in a submersion-type slice-recording chamber (Harvard Apparatus, Holliston, MA) and constantly superfused with 26°C, oxygenated Ringer's solution at a rate of 2–2.5 ml/minute.

Electrodes were pulled by a horizontal Flaming and Brown micropipette puller (model P-87; Sutter Instruments, Novato, CA) and filled with a potassium methane-sulfonate-based

NIH-PA Author Manuscript

NIH-PA Author Manuscript

NIH-PA Author Manuscript

internal solution (concentrations, in mM): 122 KCH_3SO_3, 2 $MgCl_2$, 5 EGTA, 10 NaHEPES, 1% biocytin (pH 7.4; Sigma). Cells were simultaneously filled with biocytin during recording. Slices that contained filled cells were then fixed in 4% paraformaldehyde in 0.1 M phosphate-buffered saline (PBS) solution (pH 7.4) at 4°C for 2 days. Slices were placed in 0.1% Triton X-100/PBS at room temperature for 2 hours, after rinsing with PBS (three times, 5–10–15 minutes), and were subsequently incubated with streptavidin-Alexa 488 (1:500; Invitrogen, Carlsbad, CA) at 4°C for 2 days. After incubation, slices were mounted on slides with Prolong Gold mounting medium (Invitrogen) and coverslipped.

Confocal laser scanning microscopy (CLSM) was performed as described previously (Rocher et al., 2010), with a voxel size of 0.1 $\mu m^2 \times 0.2$ μm. Each neuron's apical dendritic tree was imaged in its entirety using multiple stacks. Raw image stacks then were deconvolved using AutoDeblur (MediaCybernetics, Bethesda, MD). The final image of each neuron (Fig. 1a) was created by integrating all deconvolved stacks together using the Volume Integration and Alignment System (VIAS; Rodriguez et al., 2003). To ensure that the dendritic tree was largely complete, only cells without cut dendrites in the proximal half of the dendritic trees were used; they were never used if the apical trunk was cut. The *yz*-projection in Figure 1a demonstrates that much of the apical arbor was captured successfully.

The custom-designed software NeuronStudio (Rodriguez et al., 2006, 2008, 2009) was used for automated reconstruction of the dendritic arbor and for automated identification and shape classification of spines (Fig. 1b–d). Spine shape (mushroom, stubby, thin) was determined using criteria previously described (Rodriguez et al., 2008). Subsequent manual examination and editing reduced the incidence of false positives and negatives.

Each dendrite branch traversed a 3-D path in the image but was represented here as a one-dimensional (1-D) segment with total length equal to the branch's traversed path length. The location of each spine along the dendrite was represented by first projecting the spine head onto the dendrite, then measuring the 1-D path length from the start of the parent dendrite branch to that point (Fig. 2a).

Because basal dendrites are morphologically distinct from apical dendrites and integrate inputs somewhat differently (Spruston, 2008), we restricted the present analysis to apical dendrites. Similarly, because evidence in the CA1 field of the hippocampus suggests that spikes are generated more easily in oblique rather than terminal branches (Gasparini et al., 2004; Losonczy and Magee, 2006), we considered oblique and terminal branches separately. The oblique dendrites are distal to the primary trunk, correspond to secondary and tertiary levels of branching, and are of lower order than the apical terminal branches. Thus, whereas the terminal branches spread between the superficial parts of layer III (layer IIIa) out into layer I, the oblique branches for the most part reside in the middle portion of layer III (layer IIIb). Prior to the clustering analyses, manual inspection excluded all dendrite segments obtained from images of insufficient quality (Rodriguez et al., 2006, 2008) or with unusually high or low spine density. Branches were classified manually as either "oblique" or "apical terminal" through visual inspection. These procedures yielded 152 apical terminal branches with 23,257 spines and 128 apical oblique branches with 19,319 spines, across the seven neurons. After confocal images had been acquired and deconvolved as described above, NeuronStudio and Adobe Photoshop CS4 were used to prepare images for publication. No other digital manipulations were used.

Clustering algorithm

Unsupervised clustering algorithms avoid a priori specification of either the number of elements per cluster or the total number of clusters (MacKay, 2003). Iterative hierarchical

NIH-PA Author Manuscript

NIH-PA Author Manuscript

NIH-PA Author Manuscript

methods are one class of unsupervised clustering algorithms commonly used in pattern recognition, data mining, and computational biology (Romesburg, 1984). Hierarchical methods fall into two categories: top down and bottom up. Top-down methods begin with a single cluster containing all of the observations, then split the data into smaller clusters if specific conditions are satisfied (Murtagh, 1983; Gronau and Moran, 2007). The more common bottom-up approach begins with each individual data point ("leaf"), then iteratively combines leaves that satisfy some criteria of minimum dissimilarity among the whole set.

For our spatially distributed spine data, we chose the unweighted pair group method with arithmetic mean (UPGMA), a simple, iterative, bottom-up hierarchical clustering method that uses Euclidean distance as its minimum dissimilarity criterion. The clustering was performed separately for each dendrite branch (see Fig. 2). At the start of the clustering, the 1-D path length of each spine was represented as a leaf node. In the first iteration, two nearest leaf nodes were merged to form a higher order node located at the midpoint of the parent leaf nodes (Sokal and Michener, 1958). The merging of nearest nodes repeated in subsequent iterations, with the parent nodes being either leaf nodes or higher order nodes. Thus, as the algorithm continued, a node corresponded either to a single spine or to a group (cluster) of spines merged during previous iterations.

Figure 2b illustrates this iterative combination of nodes in the form of a dendrogram. The x-axis depicts equally spaced leaf nodes labeled 1–19, corresponding to the 19 spines on the dendritic branch shown in Figure 2a. The height along the y-axis represents the 1-D "link" distance between constituent members of the nodes created by each iteration.

By default, UPGMA iterates until all leaf nodes are combined into a single cluster with highly dispersed constituents. To stop the clustering in an objective, unsupervised way, we used a quantitative stopping criterion called the inconsistency coefficient (IC; Zahn, 1971). The IC measures the variability in link sizes of a node and its constituent nodes. The IC for the ith node of a dendrogram is given by

$$IC_i = \frac{x_i - \bar{x}_k}{\sigma_k} \quad (1)$$

where x_i is the link corresponding to the ith node, and $\bar{x}_k$ and σ_k are the mean and standard deviation of the set of links of all nodes constituting node i from k previous iterations, including x_i itself. For a node consisting of two leaves, with no lower level links against which to compare, the IC is assigned a value of 0. The IC value for a given node is low if the constituent leaf nodes are grouped together tightly and high if the constituent nodes are more dispersed.

As UPGMA progressed, we accepted new nodes only with an IC less than a prescribed cutoff, thus controlling the level of dispersal in the extracted clusters. We used an IC cutoff of 0.75, slightly higher than $1/\sqrt{2} \approx 0.71$, the minimum IC for a node with at least one nonleaf constituent. This cutoff extracted the tightest cluster groupings while ensuring that at least one leaf was included in the formation of any node. Moreover, the algorithm was allowed to group leaves into pairs but could only add one leaf at a time beyond that (Fig. 2c–e).

UPGMA is an unsupervised algorithm, so we postprocessed its results to remove clusters that were not biologically plausible. Clusters having a spine density (spines per micrometer of dendrite) smaller than the branch spine density were deemed to be unnphysical. Each unphysical cluster was reduced iteratively by pruning the one spine whose removal provided

NIH-PA Author Manuscript

NIH-PA Author Manuscript

NIH-PA Author Manuscript

the largest decrease in the length of the remaining cluster (Fig. 2f). This process continued until the spine density of the pruned cluster was greater than the branch spine density.

In our analyses, a spine cluster is defined as a group of three or more spines after the completion of UPGMA analysis and postprocessing. Spines belonging to UPGMA-identified clusters were categorized as "clustered spines." Remaining spines were categorized as "singlet spines."

Monte Carlo simulations and C score calculation

We used Monte Carlo simulations to quantify the amount of clustering observed in each dendrite branch of our data relative to the amount expected in equivalent sets of randomly placed spines. Suppose B was one such dendrite branch with 1-D length L_B and n_B spines. We also created $M = 5{,}000$ copies of B, randomly placing the n_B spines according to a uniform distribution along the length of a branch for each copy, B_i, $i = 1 \ldots M$ (Fig. 3a). UPGMA was then performed on the real branch B and on each of the randomized copies B_i. Let $Q_B \leq n_B$ be the number of clustered spines on the real branch B, and let q_i be the number of clustered spines on randomized copy B_i. We interpreted the set $\{q_i\}$ as observations of a random variable, W_B, representing the number of clustered spines extracted from each random copy of branch B.

The frequency distribution of W_B over all randomized copies was normalized to obtain a probability distribution, $P(W_B)$, of W_B. Then

$$C_B = \int_0^{Q_B} P(w_B)\,dw_B, \quad (2)$$

was the cumulative distribution function of the random variable W_B, with $0 \leq C_B \leq 1$. Hereafter called the "C-score," C_B gave the proportion of randomized copies of B that had fewer spines in clusters than was observed in the real data (Fig. 3b). A C-score close to 1 indicated that the number of clustered spines observed on the true branch B was significantly higher than expected by chance alone.

Similarly to the calculation of C_B, C-scores were also calculated for each random branch copy. By definition, these C-scores were analogous to P values with $P(W_B)$ as the underlying distribution and consequently were guaranteed to be uniformly distributed (Ewens and Grant, 2001).

Statistical analysis

The first goal of the statistical analysis was to test whether the data support the hypothesis that spine clusters occurred more frequently than was expected randomly. If so, then the second goal was to compare quantitatively the characteristics of spine clusters (e.g., cluster size, composition of spine types, spine number per cluster) that were generated by systematic biological processes with the characteristics of clusters generated randomly. In the absence of morphologic data on the precise locations of presynaptic neurons, it is impossible to predict functional significance on a cluster-by-cluster basis. Instead, we used statistical testing to distinguish individual dendritic *branches* that were "highly clustered," possessing significantly more spine clusters than were expected randomly, from branches that were "sparsely clustered." This led to our choice of the binomial test (Siegel, 1956), a test that is commonly used when grouping data into two categories. The distribution of C-scores for real and randomly generated dendritic branches was divided into two categories by introducing a threshold C_T, $0 \leq C_T \leq 1$. Branches with C-scores higher than C_T were classified as highly clustered; all other segments were considered sparsely clustered. A

NIH-PA Author Manuscript

NIH-PA Author Manuscript

NIH-PA Author Manuscript

larger threshold C_T provided a more conservative classification of a branch as highly clustered. Because C-scores for randomly generated segments were uniformly distributed, the proportions of highly clustered and sparsely clustered segments in the randomized data were $1 - C_T$ and C_T, respectively. We tested whether the proportion of highly clustered segments in the real data was significantly higher than $1 - C_T$. Under the null hypothesis that real segments were distributed no differently from random segments, the probability of an individual segment being highly clustered was $s = 1 - C_T$. Then, assuming a binomial distribution, the probability that at least m segments from a total of n segments were clustered was given by

$$P = \sum_{i=m}^{n} {}_nC_i s^i (1 - S)^{(n-i)}, \quad (3)$$

where ${}_nC_i$ is the combination operator, equal to the number of combinations of n objects taken i at a time. This gave the P value for the binomial test.

To test the null hypothesis that C-score and spine density were independent, we constructed contingency tables of C-score vs. spine density. It is reasonable to hypothesize that a high spine density would lead to a high C-score; therefore our one-sided alternative hypothesis was that C-score and spine density were positively correlated. For a given set of dendrite branches, we first determined the boundaries of the four quartiles of C-score ($Q_{1,C}$, $Q_{2,C}$, $Q_{3,C}$, $Q_{4,C}$) and spine density ($Q_{1,D}$, $Q_{2,D}$, $Q_{3,D}$, $Q_{4,D}$). Then, each cell (i,j) of the 4 × 4 contingency table was equal to the numbers of dendrite branches that were in quartile i for C score and quartile j for spine density. Thus, from a set of n branches, the expected frequency in each cell was n/16. A one-tailed χ^2 test for independence (Ewens and Grant, 2001) was used to compute the test statistic (9 df). G*Power 3 (Faul et al., 2007) was used to determine an appropriate sample size (n = 231) so that the test had 95% power to detect an effect size of 0.32, which was sufficient to detect an effect as small as a 2% deviation from the expected frequency in each cell (Cohen, 1988). From the Monte Carlo data, we repeated the χ^2 test 1,000 times with different random samples of 200 data points each. We also conducted the χ^2 test once for the C score/spine density pairs from the real data (n = 280), considering oblique and tuft branches together.

Spine cluster statistics were reported as arithmetic mean ± standard error of the mean. Statistical comparisons among highly clustered and sparsely clustered branches were performed using the Wilcoxon rank sum method after analyzing for normality using the Lilliefors test (Lilliefors, 1967). For all statistical tests, null hypotheses were rejected at $\alpha = 0.05$.

RESULTS

Seven layer III pyramidal neurons drawn from the dorsolateral PFC of three adult rhesus monkeys were imaged with a voxel size of 0.1 μm² × 0.2 μm, and dendritic branches and spines were reconstructed using automated software (Fig. 1; see Materials and Methods). We then used our clustering method (Fig. 2) and Monte Carlo simulations (Fig. 3) to analyze 128 apical oblique and 152 apical terminal branches that included 19,319 and 23,257 spines, respectively.

As detailed in Materials and Methods, the merging of spine clusters by the UPGMA algorithm was governed by the inconsistency coefficient (IC). We found that cluster extraction was largely insensitive to changes in the IC cutoff, suggesting that our algorithmic implementation of cluster extraction was robust. Figure 4 illustrates clusters identified after UPGMA but before the postprocessing. Extracted clusters were unchanged

NIH-PA Author Manuscript

NIH-PA Author Manuscript

NIH-PA Author Manuscript

for IC cutoffs ranging from 0.75 through 0.95. Above an IC cutoff of 0.95, smaller clusters were increasingly merged into larger ones. Because we wished to be conservative in identifying spine clusters, we performed our subsequent analyses with an IC cutoff of 0.75, just above the minimal IC of $1/\sqrt{2} \approx 0.71$.

The C-score is independent of spine density for randomly placed spines

It is reasonable to hypothesize that high spine density on a branch leads to a higher C-score. That is, a clustering measure might identify a group of randomly spaced spines as highly clustered simply because the spines are tightly packed (high density). We first tested whether this seemed to be true if spines were placed randomly on the branch. In particular, the Monte Carlo procedure (see Materials and Methods) created 5,000 copies of each real dendrite branch with randomly distributed spines, 1.4 million branches in all. Using 1,000 different random samples taken from the Monte Carlo population (Materials and Methods), we tested the null hypothesis that the C-score of a dendrite branch with randomly placed spines was independent of spine density. In repeating the χ^2 test on each sample, the null hypothesis of independence was rejected only 50 times. This is equal to the false-positive error rate $\alpha = 0.05$, so these results strongly support the idea that C-score is independent of spine density when spines are distributed randomly. Figure 5a illustrates C-score vs. spine density for a random sample of this population from 32 dendritic branches.

From the 280 branches of the real neurons, the null hypothesis of independence was rejected ($\chi^2 = 21.71$, $P = 0.010$). Next, by using simple linear regression analysis, we attempted to predict C-score from spine density of these data. Although the slope was significantly greater than zero (slope = 0.061; $t_{278} = 2.63$; $P = 0.0091$; $Y = 0.39 + 0.061X$), the low coefficient of determination ($r^2 = 0.024$) indicated that spine density explained very little of the observed variation in C-score (Fig. 5b).

Nonrandom clustering in cortical apical dendrites

For the remainder of this article, we use the C-score threshold C_T to define highly clustered dendrite branches as those exhibiting more clustered spines than expected randomly (see Materials and Methods). Remaining branches were considered sparsely clustered. Figure 6 presents typical examples of these branch types. Spines classified as lying in clusters are shown in pink; singlet spines that were not classified into clusters are shown in orange (Fig. 6a,b; Fig. 6c shown in black). A greater proportion of the spines was classified as lying in clusters on the highly clustered branch (Fig. 6a,c, C-score 93) than on the sparsely clustered branch (Fig. 6b,c; C-score 44). The 2-D projections (xy, yz, and xz) may be misleading, which is why it is important that the neurite reconstruction and spine detection algorithms operate in three dimensions. In particular, in 2-D projections, the traversed distance along the dendrite may appear distorted, and spines may even seem to be false positives. Looking at all three projections helps to clarify the distortions but does not completely eliminate them. Figure 6c clearly illustrates the spine locations along the length of each dendrite.

Table 1 summarizes the number of highly clustered branches as determined by two different values of the threshold C_T (0.90 and the more conservative 0.95). We tested the null hypothesis that the number of highly clustered branches observed in our data was equal to the number that was expected with randomly distributed spines. For apical terminal branches, the null hypothesis was rejected for both values of C_T (P values of 0.049 and 0.02 for $C_T = 0.90$ and 0.95 respectively). For oblique branches, the null hypothesis was not rejected for either value of C_T ($P = 0.90$ and $P = 0.88$). Thus our data support the idea that spines were highly clustered on apical terminal branches but not on oblique branches. Hereafter we use the less conservative clustering threshold $C_T = 0.90$ and yet show that

NIH-PA Author Manuscript

NIH-PA Author Manuscript

NIH-PA Author Manuscript

significant differences exist in attributes of clusters found on highly clustered and sparsely clustered branches.

Spine cluster statistics

We report spine cluster statistics on the 152 apical terminal branches, for the highly clustered and sparsely clustered groups (Table 2). As expected, the percentage of spines residing in clusters was greater for highly clustered branches compared with sparsely clustered branches ($P < 0.006$). However, the percentage of spines residing in clusters in sparsely clustered branches was similar to the percentage calculated from all 1.4 million simulated branches with randomly spaced spines (56.6%). The mean number of spines per cluster was greater on highly clustered branches ($P = 0.02$), whereas the mean cluster length was smaller ($P = 0.0037$). The cluster density (number of clusters per micrometer) was also larger on highly clustered branches ($P < 0.0001$). This statistic can be misleading, because the number of spines per cluster and cluster length varied widely. Thus, we also measured spine cluster occupancy, defined as the ratio of the total length of all clusters on a branch to the branch length. Cluster occupancy was greater on highly clustered branches ($P < 0.0001$).

Figure 7 summarizes our findings on the density of the three spine types (mushroom-shaped, stubby, thin) in apical terminal branches. We report the spine type density, equal to the number of each spine type per micrometer of branch length, for clustered and singlet (nonclustered) spines. The density of clustered spines of all types was significantly greater in highly clustered branches than in sparsely clustered branches (Fig. 7a). On highly clustered branches, the density of mushroom-shaped and stubby clustered spines was nearly twice the density on sparsely clustered branches. In contrast, the density of mushroom-shaped, stubby, or thin singlet spines did not differ between highly clustered and sparsely clustered branches (Fig. 7b).

By definition, proportionally more spines reside in clusters on highly clustered branches than on sparsely clustered branches. The larger densities of clustered spines of each type on highly clustered branches could be due to clusters being more numerous in these branches but also could be due to fundamental differences in the relative proportions of spine types within highly and sparsely clustered branches. Thus, we reexamined our shape density results after controlling for the proportion of clustered spines. After dividing the number of clustered spines of each type by the total cluster length (as opposed to the branch length), the densities of mushroom-shaped and stubby clustered spines were still significantly greater in highly clustered branches (Fig. 7c), by 43% and 56% respectively. Likewise, as alternative singlet shape densities, we divided the singlet spine count of each type by the total branch length minus cluster length. Still, there was no significant difference in the density of singlet spines of any shape for highly clustered vs. sparsely clustered branches (Fig. 7d), indicating that the increase in mushroom-shaped, stubby, and thin spines on highly clustered branches was concentrated in the clusters. Moreover, clusters on those branches had a greater increase in the density of mushroom-shaped and stubby spines than thin spines.

DISCUSSION

Neurons receive thousands of inputs and must integrate them with millisecond precision. Models have shown that neuronal processing tasks such as pattern differentiation and memory retrieval and storage could be enhanced substantially through nonlinear summation of inputs on clustered synapses (Mehta, 2004; Govindarajan et al., 2006). Empirical studies confirm that synapses activated within individual dendrite branches can achieve nonlinear summation of inputs (Larkum et al., 2009; for review see Larkum and Nevian, 2008). A recent single-synapse resolution study confirmed synchrony of network activity in adjacent spines, suggesting that spatially localized synapses are likely to group functionally

NIH-PA Author Manuscript

NIH-PA Author Manuscript

NIH-PA Author Manuscript

(Takahashi et al., 2012). Furthermore, it has been shown that learning activity patterns that induce LTP preferentially promote growth of new spines close to potentiated synapses (De Roo et al., 2008), possibly leading to clustering of functional synapses. Other experiments show that neighboring synapses on a dendritic branch during LTP induction can be coregulated (Harvey and Svoboda, 2007; Harvey et al., 2008; Govindarajan et al., 2011), again implying that spines might possibly group within a localized neighborhood. However, the existence of localized synapse clusters on multiple branches of a neuron's dendritic arbor has never been established. We have introduced a new method that analyzes spine locations along dendritic branches, classifies whether individual spines lay within clusters, and then quantifies the probability that the observed frequency of clusters occurred randomly. Our results indicate that layer III pyramidal neurons from area 46 of the monkey PFC do possess nonrandom clusters of spines on apical terminal branches, located preferentially in layers I and II and the upper part of layer III, but not oblique branches, distributed within the middle portion of layer III. We also show that the density of clustered mushroom-shaped and stubby spines is twofold greater on dendrites on which prolific clustering was found. We conclude that one or more systematic biological processes are responsible for the observed spine clusters.

Spine clustering in cortical pyramidal neurons

The layer III neurons in this study were located in area 46, a key PFC region involved in working memory tasks (Funahashi and Takeda, 2002). These tasks are short in duration and require precisely timed communication with other cortical regions. Thus, it is likely that efficient working memory processing would be facilitated by synaptic clustering on apical terminal dendrites. Our morphologic data were obtained during in vitro electrophysiological characterization of neurons from cognitively tested adult monkeys. This restricts our sample size but will allow us to test for correlations of cognitive status with neuronal structure and function as more data are collected. Even so, for $C_T = 0.90$ and $\alpha = 0.05$, our study had sufficient power to detect clustering that occurs twice as often as random 91% of the time when it exists in oblique branches and 97% in terminal branches (Cohen, 1988). Thus we propose that the spine clustering that we observed in apical terminal branches of these neurons is biologically significant and that nonrandom spine clustering in oblique branches, if it does exist, is much less common.

The present data were obtained without elicitation of synaptic plasticity or a particular learning paradigm. Spines in adult animals targeted during synaptic strengthening can be stable in vivo for days or even months (Kasai et al., 2003). At the same time, many in vitro and in vivo studies have established that a principal characteristic of dendritic spines is that they are highly plastic structures that appear and disappear and change morphological properties under both normal and pathological conditions. Thus, we propose that spine clusters can be actively maintained over long time scales but may also be highly plastic themselves.

In vitro approaches have been used previously to study the fundamental characteristics of spine motility and mechanisms underlying morphogenesis of spines, and most if not all in vitro findings have been substantiated with in vivo approaches (for a comprehensive review of this topic see Yuste, 2010). Thus the analysis of neurons that are filled during in vitro electrophysiological recordings has been used very extensively in the field. Indeed, most of the seminal findings on dendritic spines have been obtained from in vitro slice or more reduced neuronal culture systems. That said, it is true that brain slicing, a procedure that necessarily results in deafferentation and disruption of the tissue, has been reported to result in acute increases in spine number that stabilize after approximately 2 hours (Kirov et al., 1999). This report, which was limited to the hippocampus (so relevance to neocortical neurons is not known), has implications for all in vitro studies of spine number and

NIH-PA Author Manuscript

NIH-PA Author Manuscript

NIH-PA Author Manuscript

morphology, yet does not reduce the importance of in vitro data. The significance of our finding of spatial clustering of spines—an important and heretofore unappreciated capacity of cortical neurons—is not reduced by the fact that neurons were filled in vitro. In particular, we found that highly clustered branches were concentrated in the apical terminal region and that the distribution of spine shapes differed on highly clustered vs. sparsely clustered branches. It is unlikely that these findings are due merely to a slicing artifact.

Spine clusters were observed on both oblique and terminal apical branches, although the frequency on oblique branches was no different from what was expected by chance. Interestingly, oblique dendrites of CA1 pyramidal cells tend to have a lower threshold for generating local voltage spikes than apical terminal dendrites (Gasparini et al., 2004; Losonczy and Magee, 2006). Thus, we predict that prolific spine clusters on apical terminal branches of neocortical pyramidal cells facilitate dendritic spikes in order to integrate such distal synaptic input at the soma (Larkum et al., 2009). In contrast, perhaps neocortical oblique branches rely less on synapse clustering to regulate the ability of a branch to generate a voltage spike, instead using other mechanisms such as N-methyl-D-aspartate receptor-dependent regulation of A-type K^+ channels found in CA1 (Losonczy et al., 2008). Regulation of A-type K^+ channels and spine clusters within a dendrite branch might even occur simultaneously to tune the level of nonlinear input summation. Also, the apical terminal dendrites of layer III neurons are innervated mostly by inputs from other cortical regions as well as thalamic and subcortical inputs, whereas proximal apical dendrites, including proximal oblique branches, receive inputs mostly from layer IV spiny stellate neurons and from local cortical neurons (Spruston, 2008). This suggests a likely correlation between laminar input type and the presence of spine clusters.

Relevance of spine shape

The relationship between spine shape and function has been studied widely. Thin spines change into larger and more stable mushroom-shaped spines as the postsynaptic density and associated spine head volume increase (Kasai et al., 2010). It has been proposed that, during learning, thin spines are recruited to undergo LTP induction and are transformed subsequently into memory-storing mushroom-shaped spines (Bourne and Harris, 2007).Thus, the high density of mushroom-shaped spines found specifically within clusters on highly clustered branches (see Fig. 7) may be functionally significant, particularly in the context of differences in inputs to the distal tufts of dendrites, likely richer in thalamocortical and subcortical afferent axons compared with the inputs to the oblique dendrites (secondary and tertiary branching levels mostly) in the middle portion of layer III that contains a larger proportion of corticocortical afferents (Hof et al., 1995; Duan et al., 2002; Spruston, 2008). Also, because synaptic currents tend to be largest on stubby spines (Segal, 2010), the significant increase in the density of clustered stubby spines seen here further supports our prediction that nonlinear summation is enhanced on highly clustered branches and indicates that clustered stubby spines may act in concert as hot spots for dendritic depolarization. This suggests a wider role for stubby spines than typically thought (Perez-Vega et al., 2000; Diamond et al., 2006; Bourne and Harris, 2011). Our findings that the proportion of specific spine subtypes differs between highly clustered and sparsely clustered dendrites are particularly interesting because our clustering algorithms made no use of spine shape information.

Future applications of the algorithm

From an algorithmic perspective, several clustering methods could be used to locate spine clusters along a dendrite branch. A greater challenge is to establish a clustering measure that determines the probability that clusters occur purely by chance but is uncorrelated with spine density. The C-score uses statistical data randomization to meet both these criteria. In

NIH-PA Author Manuscript

NIH-PA Author Manuscript

NIH-PA Author Manuscript

simulated data with randomly spaced spines, the C-score is independent (consequently uncorrelated) of spine density (Fig. 5a), but, in the real data, spine density and C-score were weakly correlated (Fig. 5b), further evidence that the clustering observed experimentally has a nonrandom and systematic cause.

With sufficient morphologic data, our C-score could test a variety of hypotheses on spine clustering. Variations in the degree of spine clustering across neuronal populations and multiple brain regions could help to decipher connectivity patterns in neuronal circuits (Chklovskii et al., 2004). Differences in spine clustering between perfused tissue and acute slices (Kirov et al., 1999) could also be assessed. A previous study showed that large spines were farther from one another than smaller spines (Konur et al., 2003); this could be tested in our data by analyzing spine volumes, which also could be used to infer synaptic strength (Matsuzaki et al., 2004; Kopec et al., 2006; Harvey and Svoboda, 2007; Zito et al., 2009). The C-score could also quantify the level of spine clustering before and after LTP induction (Harvey and Svoboda, 2007; De Roo et al., 2008) or other learning paradigms. Finally, dendrites and spines undergo substantial morphologic dystrophy in aging (Cupp and Uemura, 1980; Uemura, 1980; de Brabander et al., 1998; Peters et al., 1998, 2001; Kajkowski et al., 2001; Duan et al., 2003; Dickstein et al., 2007; Kabaso et al., 2009; Hara et al., 2011) and in neurodegenerative disorders (Hof et al., 1995; Anderton et al., 1998; Hao et al., 2006, 2007; Knobloch and Mansuy, 2008; Dumitriu et al., 2010; Luebke et al., 2010; Rocher et al., 2010; Bloss et al., 2011). If synaptic connections were to reorganize in an attempt to compensate for these morphologic changes, spine clusters might become more prominent in one region of a neuron than in another. The data presented here provide an important baseline for testing such hypotheses.

Acknowledgments

We thank Dr. Yongchao Ge for helpful discussion and the Mount Sinai School of Medicine for additional support.

Grant Sponsor: National Institutes of Health; Grant numbers: MH071818, AG035071, AG025062, and AG00001.

LITERATURE CITED

Anderton BH, Callahan L, Coleman P, Davies P, Flood D, Jicha GA, Ohm T, Weaver C. Dendritic changes in Alzheimer's disease and factors that may underlie these changes. Prog Neurobiol. 1998; 55:595–609. [PubMed: 9670220]

Bloss EB, Morrison JH, Hof PR, Dickstein DL. Influence of aging and neurodegeneration on dendritic spine morphology. Translational Neurosci. 2011; 2:49–60.

Bourne J, Harris KM. Do thin spines learn to be mushroom spines that remember? Curr Opin Neurobiol. 2007; 17:381–386. [PubMed: 17498943]

Bourne JN, Harris KM. Coordination of size and number of excitatory and inhibitory synapses results in a balanced structural plasticity along mature hippocampal CA1 dendrites during LTP. Hippocampus. 2011; 21:354–373. [PubMed: 20101601]

Chang YM, Rosene DL, Killiany RJ, Mangiamele LA, Luebke JI. Increased action potential firing rates of layer 2/3 pyramidal cells in the prefrontal cortex are significantly related to cognitive performance in aged monkeys. Cereb Cortex. 2005; 15:409–418. [PubMed: 15749985]

Chklovskii DB, Mel BW, Svoboda K. Cortical rewiring and information storage. Nature. 2004; 431:782–788. [PubMed: 15483599]

Cohen, J. Statistical power analysis for the behavioral sciences. Hillsdale, NJ: Lawrence Erlbaum Associates; 1988. p. 567xxi

Cupp CJ, Uemura E. Age-related-changes in prefrontal cortex of *Macaca mulatta*—quantitative-analysis of dendritic branching patterns. Exp Neurol. 1980; 69:143–163. [PubMed: 6771151]

NIH-PA Author Manuscript

NIH-PA Author Manuscript

NIH-PA Author Manuscript

de Brabander JM, Kramers RJK, Uylings HBM. Layer-specific dendritic regression of pyramidal cells with ageing in the human prefrontal cortex. Eur J Neurosci. 1998; 10:1261–1269. [PubMed: 9749780]

De Roo M, Klauser P, Muller D. LTP promotes a selective long-term stabilization and clustering of dendritic spines. PLoS Biol. 2008; 6:e219. [PubMed: 18788894]

Diamond DM, Campbell AM, Park CR, Woodson JC, Conrad CD, Bachstetter AD, Mervis RF. Influence of predator stress on the consolidation versus retrieval of long-term spatial memory and hippocampal spinogenesis. Hippocampus. 2006; 16:571–576. [PubMed: 16741974]

Dickstein DL, Kabaso D, Rocher AB, Luebke JI, Wearne SL, Hof PR. Changes in the structural complexity of the aged brain. Aging Cell. 2007; 6:275–284. [PubMed: 17465981]

Duan H, Wearne L, Morrison JH, Hof PR. Quantitative analysis of the dendritic morphology of corticocortical projection neurons in the macaque monkey association cortex. Neuroscience. 2002; 114:349–359. [PubMed: 12204204]

Duan H, Wearne SL, Rocher AB, Macedo A, Morrison JH, Hof PR. Age-related dendritic and spine changes in corticocortically projecting neurons in macaque monkeys. Cereb Cortex. 2003; 13:950–961. [PubMed: 12902394]

Dumitriu D, Hao J, Hara Y, Kaufmann J, Janssen WG, Lou W, Rapp PR, Morrison JH. Selective changes in thin spine density and morphology in monkey prefrontal cortex correlate with aging-related cognitive impairment. J Neurosci. 2010; 30:7507–7515. [PubMed: 20519525]

Dumitriu D, Rodriguez A, Morrison JH. High-throughput, detailed, cell-specific neuroanatomy of dendritic spines using microinjection and confocal microscopy. Nat Protoc. 2011; 6:1391–1411. [PubMed: 21886104]

Ewens, WJ.; Grant, G. Statistical methods in bioinformatics: an introduction. New York: Springer; 2001. p. 476xix

Faul F, Erdfelder E, Lang AG, Buchner A. G*Power 3: a flexible statistical power analysis program for the social, behavioral, and biomedical sciences. Behav Res Methods. 2007; 39:175–191. [PubMed: 17695343]

Funahashi S, Takeda K. Information processes in the primate prefrontal cortex in relation to working memory processes. Rev Neurosci. 2002; 13:313–345. [PubMed: 12542260]

Gasparini S, Migliore M, Magee JC. On the initiation and propagation of dendritic spikes in CA1 pyramidal neurons. J Neurosci. 2004; 24:11046–11056. [PubMed: 15590921]

Gordon U, Polsky A, Schiller J. Plasticity compartments in basal dendrites of neocortical pyramidal neurons. J Neurosci. 2006; 26:12717–12726. [PubMed: 17151275]

Govindarajan A, Kelleher RJ, Tonegawa S. A clustered plasticity model of long-term memory engrams. Nat Rev Neurosci. 2006; 7:575–583. [PubMed: 16791146]

Govindarajan A, Israely I, Huang SY, Tonegawa S. The dendritic branch is the preferred integrative unit for protein synthesis-dependent LTP. Neuron. 2011; 69:132–146. [PubMed: 21220104]

Gronau I, Moran S. Optimal implementations of UPGMA and other common clustering algorithms. Inform Process Lett. 2007; 104:205–210.

Hao J, Rapp PR, Leffler AE, Leffler SR, Janssen WG, Lou W, McKay H, Roberts JA, Wearne SL, Hof PR, Morrison JH. Estrogen alters spine number and morphology in prefrontal cortex of aged female rhesus monkeys. J Neurosci. 2006; 26:2571–2578. [PubMed: 16510735]

Hao J, Rapp PR, Janssen WG, Lou W, Lasley BL, Hof PR, Morrison JH. Interactive effects of age and estrogen on cognition and pyramidal neurons in monkey prefrontal cortex. Proc Natl Acad Sci U S A. 2007; 104:11465–11470. [PubMed: 17592140]

Hara Y, Park CS, Janssen WG, Punsoni M, Rapp PR, Morrison JH. Synaptic characteristics of dentate gyrus axonal boutons and their relationships with aging, menopause, and memory in female rhesus monkeys. J Neurosci. 2011; 31:7737–7744. [PubMed: 21613486]

Harvey CD, Svoboda K. Locally dynamic synaptic learning rules in pyramidal neuron dendrites. Nature. 2007; 450:1195–1200. [PubMed: 18097401]

Harvey CD, Yasuda R, Zhong H, Svoboda K. The spread of Ras activity triggered by activation of a single dendritic spine. Science. 2008; 321:136–140. [PubMed: 18556515]

Hof PR, Nimchinsky EA, Morrison JH. Neurochemical phenotype of corticocortical connections in the macaque monkey: quantitative analysis of a subset of neurofilament protein-immunoreactive

NIH-PA Author Manuscript

NIH-PA Author Manuscript

NIH-PA Author Manuscript

projection neurons in frontal, parietal, temporal, and cingulate cortices. J Comp Neurol. 1995; 362:109–133. [PubMed: 8576425]

Kabaso D, Coskren PJ, Henry BI, Hof PR, Wearne SL. The electrotonic structure of pyramidal neurons contributing to prefrontal cortical circuits in macaque monkeys is significantly altered in aging. Cereb Cortex. 2009; 19:2248–2268. [PubMed: 19150923]

Kajkowski EM, Lo CF, Ning XP, Walker S, Sofia HJ, Wang W, Edris W, Chanda P, Wagner E, Vile S, Ryan K, McHendry-Rinde B, Smith SC, Wood A, Rhodes KJ, Kennedy JD, Bard J, Jacobsen JS, Ozenberger BA. Beta-amyloid peptide-induced apoptosis regulated by a novel protein containing a G protein activation module. J Biol Chem. 2001; 276:18748–18756. [PubMed: 11278849]

Kasai H, Matsuzaki M, Noguchi J, Yasumatsu N, Nakahara H. Structure–stability–function relationships of dendritic spines. Trend Neurosci. 2003; 26:360–368. [PubMed: 12850432]

Kasai H, Fukuda M, Watanabe S, Hayashi-Takagi A, Noguchi J. Structural dynamics of dendritic spines in memory and cognition. Trends Neurosci. 2010; 33:121–129. [PubMed: 20138375]

Kerr JND, Denk W. Imaging in vivo: watching the brain in action. Nat Rev Neurosci. 2008; 9:195–205. [PubMed: 18270513]

Kirov SA, Sorra KE, Harris KM. Slices have more synapses than perfusion-fixed hippocampus from both young and mature rats. J Neurosci. 1999; 19:2876–2886. [PubMed: 10191305]

Knobloch M, Mansuy IM. Dendritic spine loss and synaptic alterations in Alzheimer's disease. Mol Neurobiol. 2008; 37:73–82. [PubMed: 18438727]

Konur S, Rabinowitz D, Fenstermaker VL, Yuste R. Systematic regulation of spine sizes and densities in pyramidal neurons. J Neurobiol. 2003; 56:95–112. [PubMed: 12838576]

Kopec CD, Li B, Wei W, Boehm J, Malinow R. Glutamate receptor exocytosis and spine enlargement during chemically induced long-term potentiation. J Neurosci. 2006; 26:2000–2009. [PubMed: 16481433]

Larkum ME, Nevian T. Synaptic clustering by dendritic signalling mechanisms. Curr Opin Neurobiol. 2008; 18:321–331. [PubMed: 18804167]

Larkum ME, Zhu JJ, Sakmann B. Dendritic mechanisms underlying the coupling of the dendritic with the axonal action potential initiation zone of adult rat layer 5 pyramidal neurons. J Physiol. 2001; 533:447–466. [PubMed: 11389204]

Larkum ME, Nevian T, Sandler M, Polsky A, Schiller J. Synaptic integration in tuft dendrites of layer 5 pyramidal neurons: a new unifying principle. Science. 2009; 325:756–760. [PubMed: 19661433]

Lemmens MAM, Steinbusch HWM, Rutten BPF, Schmitz C. Advanced microscopy techniques for quantitative analysis in neuromorphology and neuropathology research: current status and requirements for the future. J Chem Neuroanat. 2010; 40:199–209. [PubMed: 20600825]

Lilliefors HW. On Kolmogorov-Smirnov test for normality with mean and variance unknown. J Am Statist Assoc. 1967; 62:399.

Livet J, Weissman TA, Kang HN, Draft RW, Lu J, Bennis RA, Sanes JR, Lichtman JW. Transgenic strategies for combinatorial expression of fluorescent proteins in the nervous system. Nature. 2007; 450:56–62. [PubMed: 17972876]

Losonczy A, Magee JC. Integrative properties of radial oblique dendrites in hippocampal CA1 pyramidal neurons. Neuron. 2006; 50:291–307. [PubMed: 16630839]

Losonczy A, Makara JK, Magee JC. Compartmentalized dendritic plasticity and input feature storage in neurons. Nature. 2008; 452:436–441. [PubMed: 18368112]

Luebke JI, Amatrudo JM. Age-related increase of sI(AHP) in prefrontal pyramidal cells of monkeys: relationship to cognition. Neurobiol Aging. 2010

Luebke JI, Chang YM. Effects of aging on the electrophysiological properties of layer 5 pyramidal cells in the monkey prefrontal cortex. Neuroscience. 2007; 150:556–562. [PubMed: 17981400]

Luebke JI, Weaver CM, Rocher AB, Rodriguez A, Crimins JL, Dickstein DL, Wearne SL, Hof PR. Dendritic vulnerability in neurodegenerative disease: insights from analyses of cortical pyramidal neurons in transgenic mouse models. Brain Struct Funct. 2010; 214:181–199. [PubMed: 20177698]

MacKay, DJC. Information theory, inference, and learning algorithms. New York: Cambridge University Press; 2003. p. 628xii

NIH-PA Author Manuscript

NIH-PA Author Manuscript

NIH-PA Author Manuscript

Matsuzaki M, Honkura N, Ellis-Davies GCR, Kasai H. Structural basis of long-term potentiation in single dendritic spines. Nature. 2004; 429:761–766. [PubMed: 15190253]

Mehta MR. Cooperative LTP can map memory sequences on dendritic branches. Trends Neurosci. 2004; 27:69–72. [PubMed: 15106650]

Meijering E. Neuron tracing in perspective. Cytometry. 2010; 77A:693–704. [PubMed: 20583273]

Murayama M, Perez-Garci E, Luscher HR, Larkum ME. Fiberoptic system for recording dendritic calcium signals in layer 5 neocortical pyramidal cells in freely moving rats. J Neurophysiol. 2007; 98:1791–1805. [PubMed: 17634346]

Murtagh F. A survey of recent advances in hierarchicalclustering algorithms. Comput J. 1983; 26:354–359.

Nikolenko V, Poskanzer KE, Yuste R. Two-photon photostimulation and imaging of neural circuits. Nat Methods. 2007; 4:943–950. [PubMed: 17965719]

Perez-Vega MI, Feria-Velasco A, Gonzalez-Burgos I. Prefrontocortical serotonin depletion results in plastic changes of prefrontocortical pyramidal neurons, underlying a greater efficiency of short-term memory. Brain Res Bull. 2000; 53:291–300. [PubMed: 11113583]

Peters A, Sethares C, Moss MB. The effects of aging on layer 1 in area 46 of prefrontal cortex in the rhesus monkey. Cereb Cortex. 1998; 8:671–684. [PubMed: 9863695]

Peters A, Moss MB, Sethares C. The effects of aging on layer 1 of primary visual cortex in the rhesus monkey. Cereb Cortex. 2001; 11:93–103. [PubMed: 11208664]

Petreanu L, Huber D, Sobczyk A, Svoboda K. Channelrhodopsin-2-assisted circuit mapping of long-range callosal projections. Nat Neurosci. 2007; 10:663–668. [PubMed: 17435752]

Poirazi P, Mel BW. Impact of active dendrites and structural plasticity on the memory capacity of neural tissue. Neuron. 2001; 29:779–796. [PubMed: 11301036]

Poirazi P, Brannon T, Mel BW. Pyramidal neuron as twolayer neural network. Neuron. 2003; 37:989–999. [PubMed: 12670427]

Polsky A, Mel BW, Schiller J. Computational subunits in thin dendrites of pyramidal cells. Nat Neurosci. 2004; 7:621–627. [PubMed: 15156147]

Rocher AB, Crimins JL, Amatrudo JM, Kinson MS, Todd-Brown MA, Lewis J, Luebke JI. Structural and functional changes in tau mutant mice neurons are not linked to the presence of NFTs. Exp Neurol. 2010; 223:385–393. [PubMed: 19665462]

Rodriguez A, Ehlenberger D, Kelliher K, Einstein M, Henderson SC, Morrison JH, Hof PR, Wearne SL. Automated reconstruction of three-dimensional neuronal morphology from laser scanning microscopy images. Methods. 2003; 30:94–105. [PubMed: 12695107]

Rodriguez A, Ehlenberger DB, Hof PR, Wearne SL. Rayburst sampling, an algorithm for automated threedimensional shape analysis from laser scanning microscopy images. Nat Protoc. 2006; 1:2152–2161. [PubMed: 17487207]

Rodriguez A, Ehlenberger DB, Dickstein DL, Hof PR, Wearne SL. Automated three-dimensional detection and shape classification of dendritic spines from fluorescence microscopy images. Plos One. 2008; 3:e1997. [PubMed: 18431482]

Rodriguez A, Ehlenberger DB, Hof PR, Wearne SL. Three-dimensional neuron tracing by voxel scooping. J Neurosci Methods. 2009; 184:169–175. [PubMed: 19632273]

Romesburg, HC. Cluster analysis for researchers. Belmont, CA: Lifetime Learning Publications; 1984. p. 334xiii

Segal M. Dendritic spines, synaptic plasticity and neuronal survival: activity shapes dendritic spines to enhance neuronal viability. Eur J Neurosci. 2010; 31:2178–2184. [PubMed: 20550565]

Siegel, S. Nonparametric statistics for the behavioral sciences. New York: McGraw-Hill; 1956. p. 312

Sokal RR, Michener CD. A statistical method for evaluating systematic relationships. Univ Kansas Sci Bull. 1958; 38:1409–1438.

Spruston N. Pyramidal neurons: dendritic structure and synaptic integration. Nat Rev Neurosci. 2008; 9:206–221. [PubMed: 18270515]

Takahashi N, Kitamura K, Matsuo N, Mayford M, Kano M, Matsuki N, Ikegaya Y. Locally synchronized synaptic inputs. Science. 2012; 335:353–356. [PubMed: 22267814]

NIH-PA Author Manuscript

NIH-PA Author Manuscript

NIH-PA Author Manuscript

Uemura E. Age-related-changes in prefrontal cortex of *Macaca mulatta*—synaptic density. Exp Neurol. 1980; 69:164–172. [PubMed: 6771152]

Wickersham IR, Lyon DC, Barnard RJO, Mori T, Finke S, Conzelmann KK, Young JAT, Callaway EM. Monosynaptic restriction of transsynaptic tracing from single, genetically targeted neurons. Neuron. 2007; 53:639–647. [PubMed: 17329205]

Wilt BA, Burns LD, Ho ETW, Ghosh KK, Mukamel EA, Schnitzer MJ. Advances in light microscopy for neuroscience. Annu Rev Neurosci. 2009; 32:435–506. [PubMed: 19555292]

Yuste, R. Dendritic spines. Cambridge, MA: MIT Press; 2010. p. 264xiv

Zahn CT. Graph-theoretical methods for detecting and describing gestalt clusters. IEEE Trans Comput C. 1971; 20:68–86.

Zito K, Scheuss V, Knott G, Hill T, Svoboda K. Rapid functional maturation of nascent dendritic spines. Neuron. 2009; 61:247–258. [PubMed: 19186167]

NIH-PA Author Manuscript
NIH-PA Author Manuscript
NIH-PA Author Manuscript

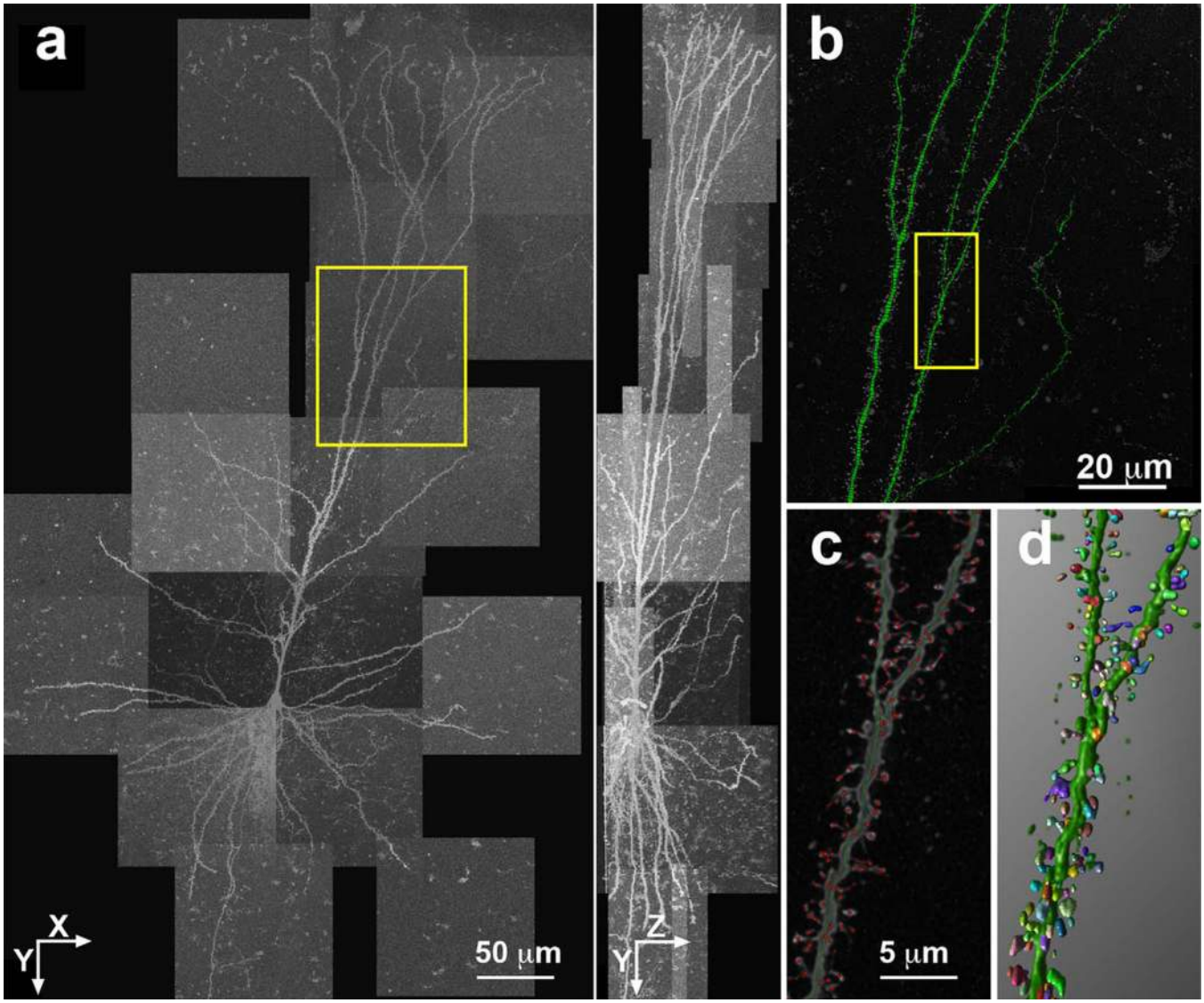

Figure 1.

Imaging and automated reconstruction of neurons. **a:** The *xy*- and *yz*-projections of deconvolved CLSM image stacks of a layer III pyramidal neuron from area 46 of a rhesus monkey, integrated with VIAS. **b:** Detail of automated reconstruction of dendritic trees using NeuronStudio. This region is boxed in *a*. The box in *b* denotes the region shown in detail in *c,d*. **c:** Dendrite centerline (green line) and spine detection (red dots) using NeuronStudio, superimposed on the deconvolved data. **d:** 3-D representation of the dendrite branch and spine reconstruction shown in *c*. Scale bars = 50 μm in *a*; 20 μm in *b*; 5 μm in *c* (applies to *c,d*).

NIH-PA Author Manuscript
NIH-PA Author Manuscript
NIH-PA Author Manuscript

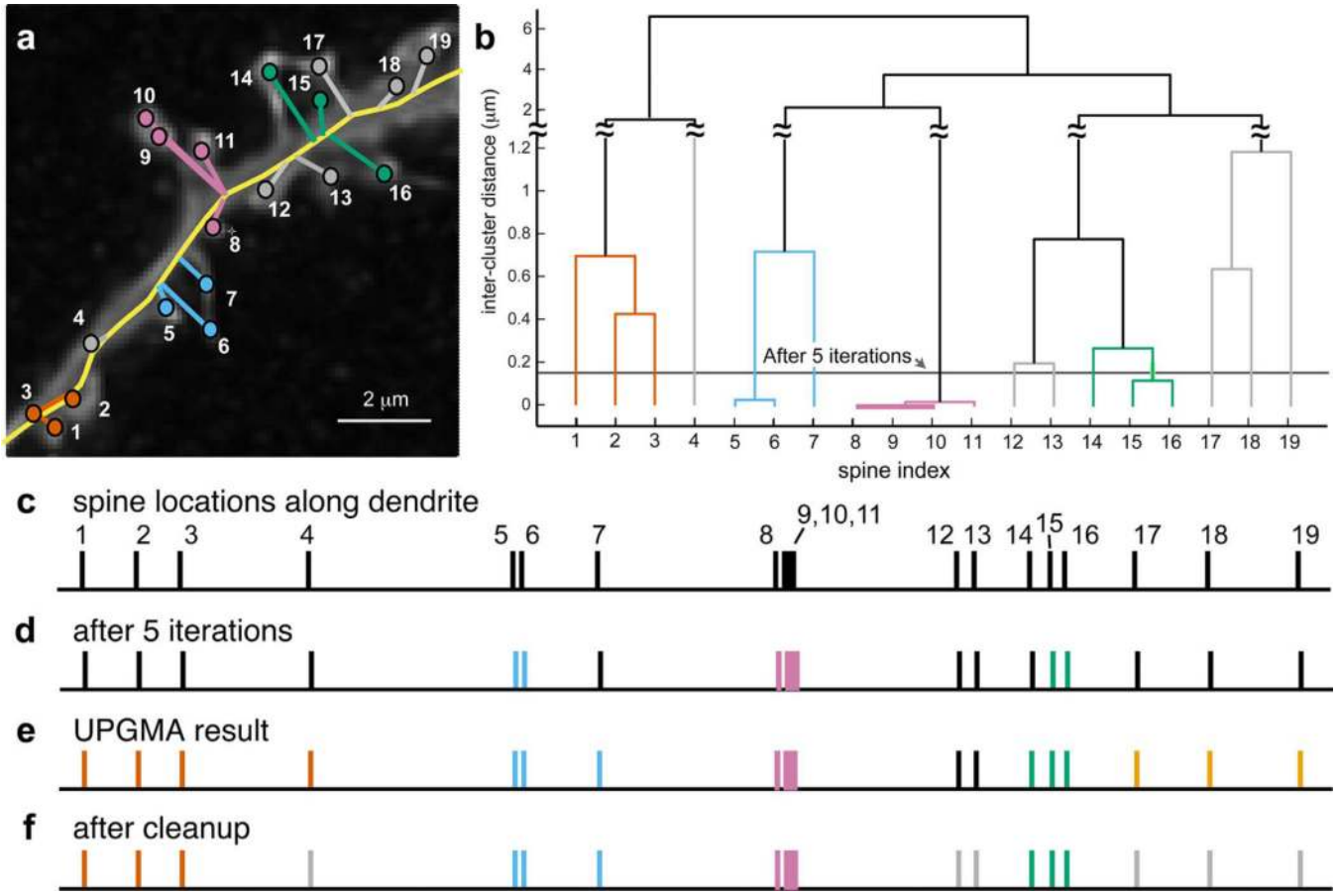

Figure 2.

Illustration of UPGMA clustering algorithm. **a:** Nineteen spines identified automatically along a segment of dendrite branch, superimposed on the *xy*-projection of the deconvolved CLSM image. Each spine head is shown as a colored circle, with a straight line illustrating its projection onto the dendritic centerline (yellow). Colors signify the final clusters determined by the algorithm shown in *f*; spines not belonging to a cluster are shown in gray. **b:** Dendrogram of the full UPGMA process. The *x*-axis depicts equally spaced leaf nodes corresponding to the spines in *a*; the height along the *y*-axis represents the 1-D distance between constituent members of the nodes created at each iteration. Colors correspond to the final cluster groupings. Groupings that violate the inconsistency coefficient (see Materials and Methods), shown in black, were not performed. **c:** Schematic representation of 1-D spine locations along the dendrite. **d:** Spine clusters identified after five iterations of UPGMA (gray horizontal line in *b*). Colored spines have already been merged into groupings; black spines have not yet been classified. **e:** Cluster groupings identified at the termination of the UPGMA algorithm, before pruning unrealistic clusters. **f:** Final clustering results, after pruning clusters with the density-based cutoff (see Materials and Methods). Spines identified within each cluster are shown in a single color and are classified as "clustered spines" for subsequent analyses. Remaining spines (shown in gray) are classified as singlets. Scale bar = 2 µm in *a*.

NIH-PA Author Manuscript
NIH-PA Author Manuscript
NIH-PA Author Manuscript

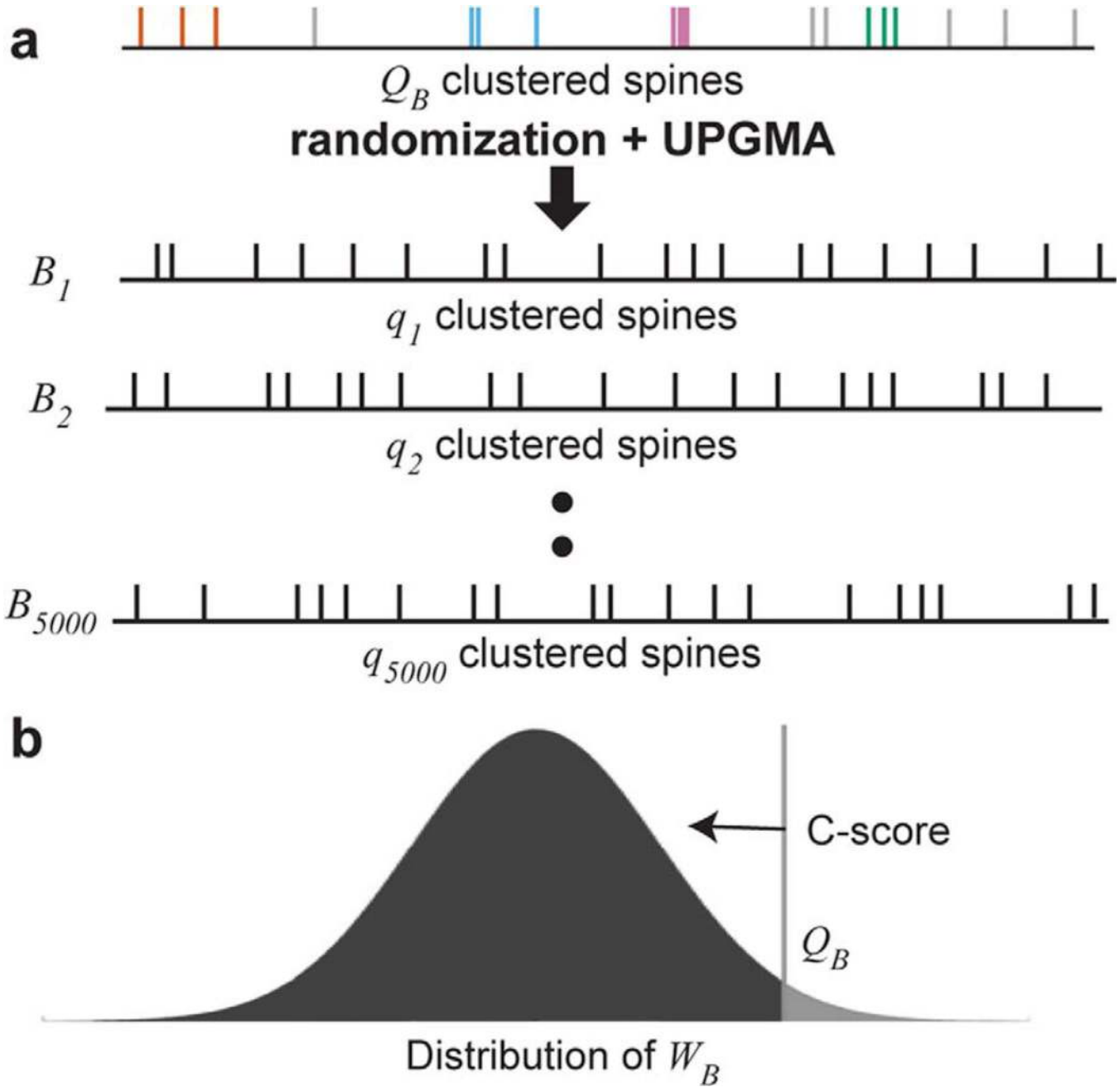

Figure 3.

Randomization method to evaluate degree of clustering in data. a: Final UPGMA result from Figure 2f, as a representative branch to illustrate randomization. Each section of length L_B and n_B spines was analyzed via UPGMA, resulting in Q_B spines grouped into clusters. Then, $M = 5{,}000$ copies of the branch were made, each having length L_B and randomized locations of the n_B spines. Random branch copies are labeled as B_i, with $i = 1, 2 \ldots M$, and the number of spines in clusters for each random copy is labeled q_i. **b:** The M q_i values make up an approximately normal distribution. The C-score for each real branch gave the percentage of this distribution that is smaller than C_T.

NIH-PA Author Manuscript
NIH-PA Author Manuscript
NIH-PA Author Manuscript

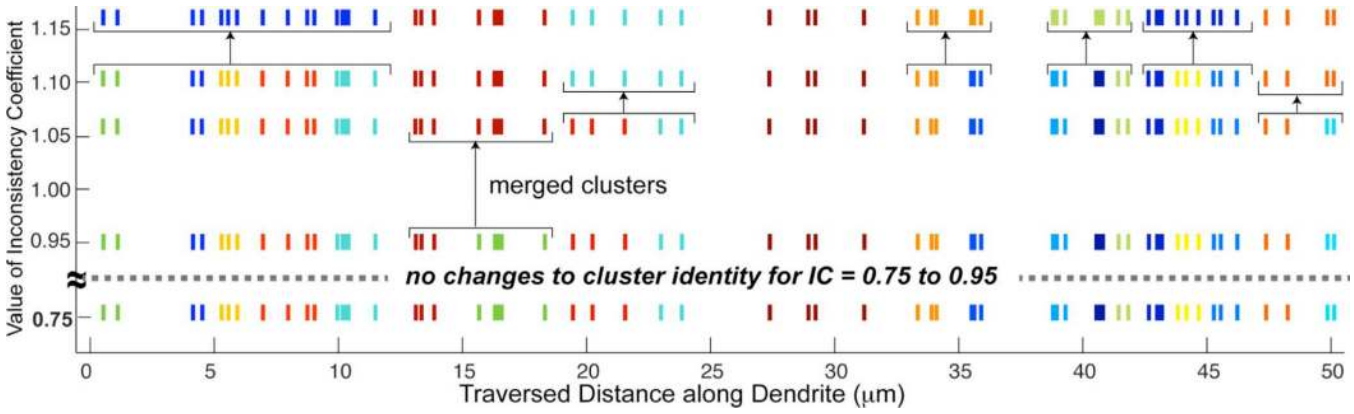

Figure 4.

Cluster groupings were largely insensitive to the inconsistency coefficient (IC) cutoff. The x-axis illustrates the 1-D locations of 62 spines along a 50-μm length of dendrite. Each color signifies a group of spines merged into a single cluster by UPGMA, using the IC criterion cutoffs shown along the y-axis. Cluster groupings were identical for IC cutoffs from 0.75 to 0.95. Above 0.95, smaller clusters were merged into larger ones, as denoted by brackets and arrows.

NIH-PA Author Manuscript

NIH-PA Author Manuscript

NIH-PA Author Manuscript

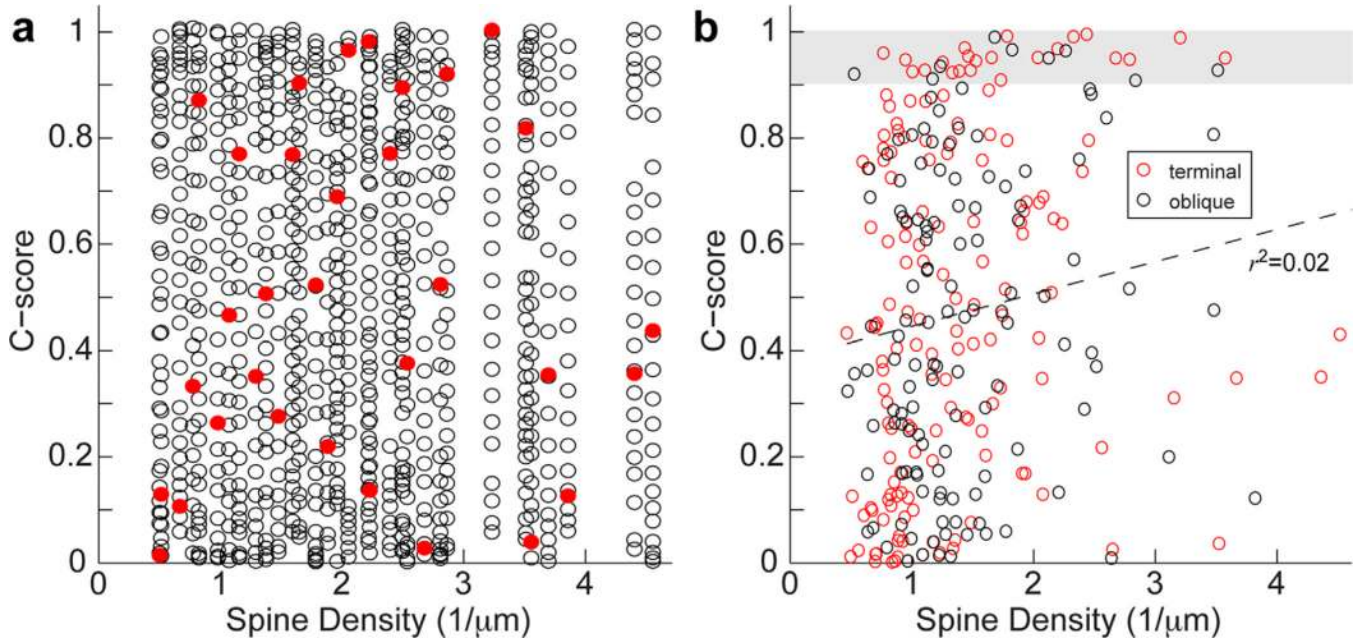

Figure 5.

C-score vs. spine density for randomized and real data. **a:** Scatterplot of C-score vs. spine density for randomized copies of 32 dendrite branches. Each red circle denotes the clustering result of a branch from the real data, a subset of the data from *b*. Open black circles show the C-score for 50 randomized copies of each of these branches. For these randomized data, C-score was independent of spine density. **b:** Scatterplot of C-score vs. spine density for all 280 dendrite branches from the real imaged neurons. Red circles denote apical terminal branches, and black circles denote oblique branches. The dashed line shows the best-fit linear regression ($r^2 = 0.02$), and the gray region represents branches that were classified as "highly clustered."

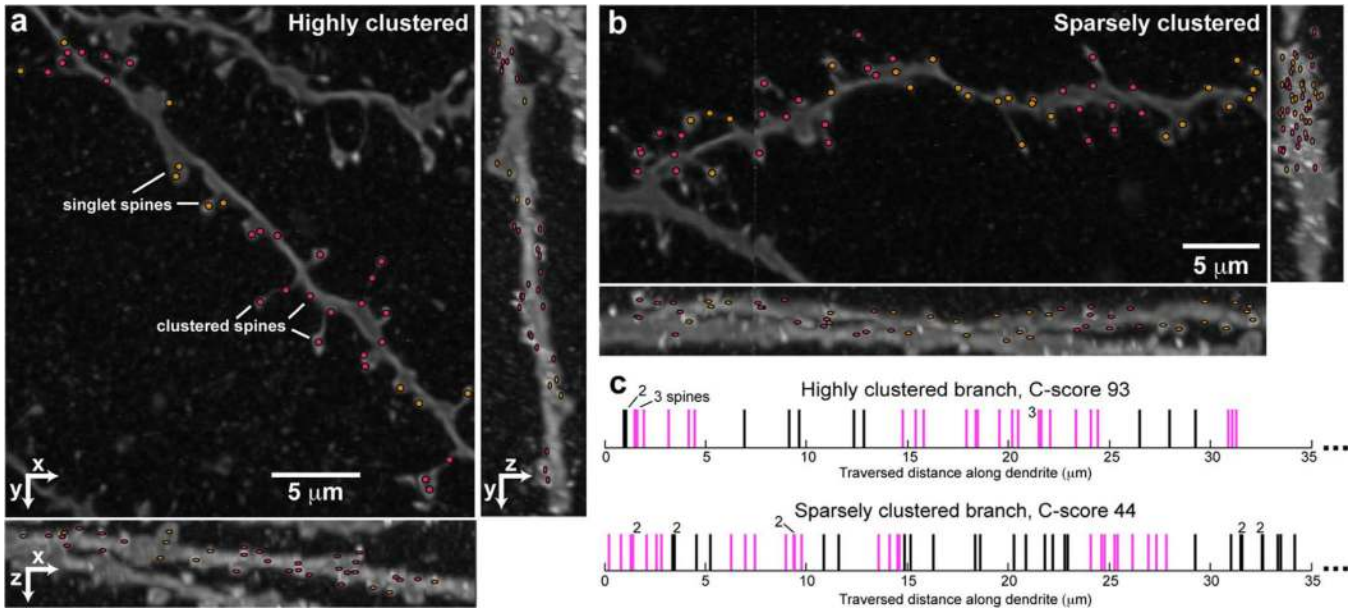

Figure 6.

Examples of typical highly clustered and sparsely clustered branches. Shown are *xy*-, *yz*-, and *xz*-projections of 35-μm segments of a highly clustered branch (**a**) and a sparsely clustered branch (**b**). Spines classified as belonging in clusters are shown in pink; nonclustered "singlet" spines are shown in black. **c:** Positions of spines on these branches, as the 1-D traversed distance along the dendritic centerline. Clustered spines are shown in pink, singlet spines in black. Scale bars = 5 μm.

NIH-PA Author Manuscript NIH-PA Author Manuscript NIH-PA Author Manuscript

NIH-PA Author Manuscript
NIH-PA Author Manuscript
NIH-PA Author Manuscript

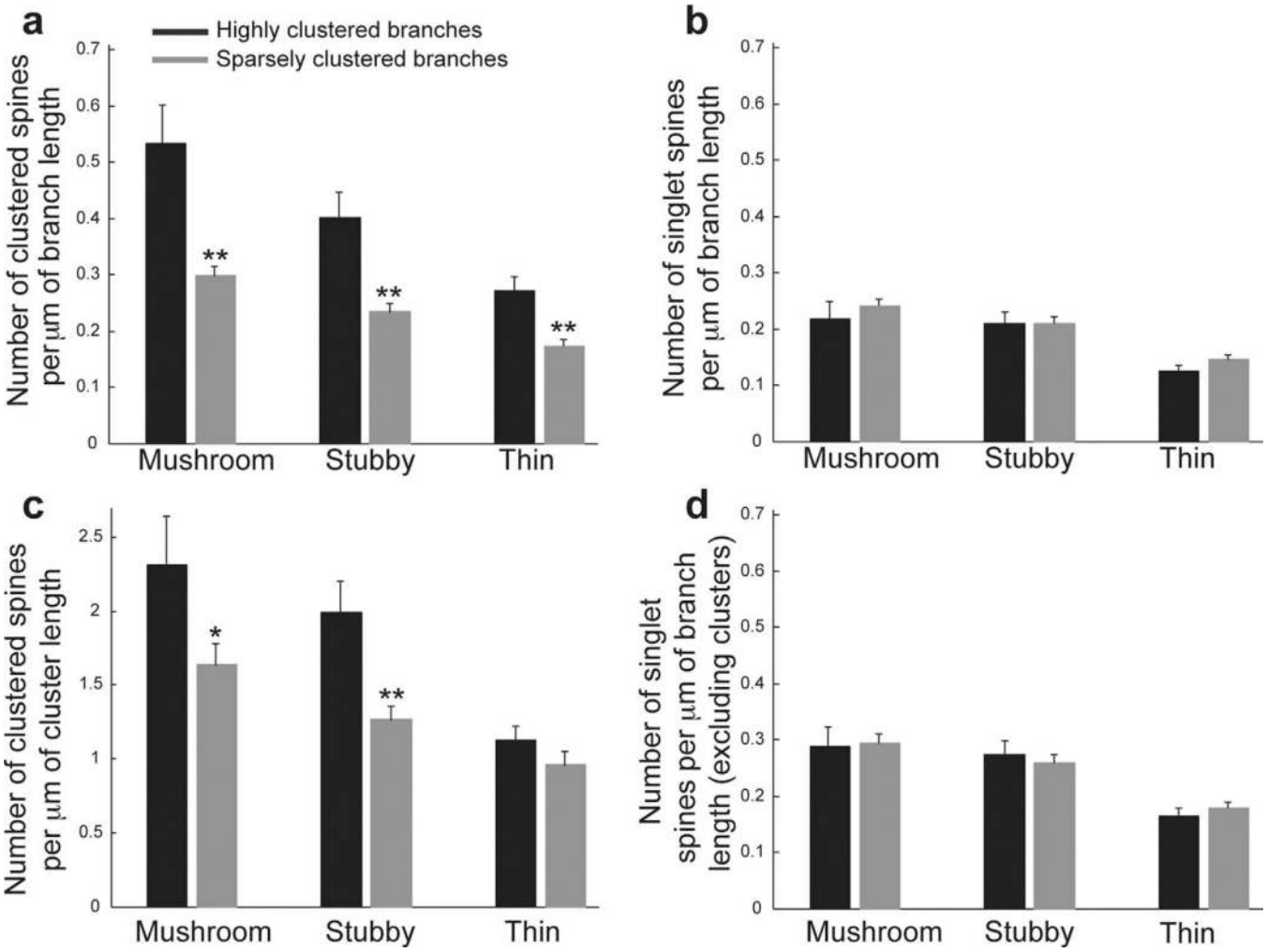

Figure 7.

Density of spine shapes in highly and sparsely clustered branches. The figure shows the density of mushroom-shaped, thin, and stubby clustered spines per unit branch length (**a**); singlet spines per unit branch length (**b**); clustered spines, normalized by the total length of dendrite over which clusters reside (**c**); and singlet spines, normalized by the length of dendrite over which singlets reside (**d**). Bars show the mean and standard error of the mean. Black and gray bars represent highly clustered (n = 22) and sparsely clustered (n = 130) branches, respectively. *P < 0.05, **P < 0.01.

NIH-PA Author Manuscript

NIH-PA Author Manuscript

NIH-PA Author Manuscript

TABLE 1

Numbers of Highly Clustered Branches vs. C-Score Clustering Threshold

	Apical terminal branches (n = 152)		Oblique branches (n = 128)	
Threshold C_T	Highly clustered branches	*P* value	Highly clustered branches	*P* value
0.9	22	0.049	9	0.90
0.95	14	0.02	4	0.88

NIH-PA Author Manuscript

NIH-PA Author Manuscript

NIH-PA Author Manuscript

TABLE 2

Cluster Statistics in Apical Terminal Branches

	Highly clustered	Sparsely clustered	*P* value
Spines in clusters (%)	69.51 ± 5.08	53.82 ± 8.1221	<0.0001
Spines per cluster	3.54 ± 0.12	3.43 ± 0.18	0.006
Cluster length (μm)	0.80 ± 0.38	1.13 ± 0.50	0.0037
Cluster density (/μm)	0.35 ± 0.14	0.20 ± 0.11	<0.0001
Cluster occupancy	0.24 ± 0.04	0.18 ± 0.04	<0.0001
Spine density (/μm)	1.818 ± 0.74	1.302 ± 0.71	0.0021